An Experimental Investigation of Direct Laser Metal Deposition Additive Manufacturing for Inconel 718 Superalloy

Mahmoud Moradi [1, 2*], Zeynab Pourmand [2], Arman Hasani [2], Mojtaba Karami Moghadam [2], Amir Hosein Sakhaei [3], Mahmood Shafiee [3], Jonathan Lawrence [4]

[1] School of Mechanical, Aerospace and Automotive Engineering, Faculty of Engineering, Environment and Computing, Coventry University, Gulson Road, Coventry CV1 2JH, United Kingdom
[2] Department of Mechanical Engineering, Faculty of Engineering, Malayer University, Malayer, Iran
[3] Mechanical Engineering Group, School of Engineering, University of Kent, Canterbury CT2 7NL, United Kingdom
[4] School of Engineering, Arden University, Arden House, Middlemarch Park, Coventry CV3 4FJ, United Kingdom

Abstract

In this study, Direct Laser Metal Deposition (DLMD) technique is adopted for the additive manufacturing of Inconel 718 Superalloy. To conduct the experiments, a 1 kW fiber laser with a coaxial nozzle head is used. The effects of scanning speed (for two values of 2.5 and 5 mm/s) as well as powder feed rate (for two values of 17.94 and 28.52 gr/min) on the process were investigated. Characteristics of the 3D printed wall specimens such as the geometrical dimensions (width and height), microstructure observations, and the micro-hardness were obtained. In order to study the stability of the 3D manufactured walls, the height stability was considered for the investigation. Optical microscopy (OM), Field Emission Electron Microscopy (FE-SEM), Energy Dispersive X-ray Spectroscopy (EDS), and mapping analysis were performed to derive the microstructural features of the additive manufactured samples. The Vickers micro-hardness test is used to evaluate the hardness distributions of additively manufactured parts. Catchment concept of the powder in DLMD process is used for explaining different trends of the process. Results indicated that, by decreasing the scanning speed, the width and height of the deposited layer increase. The average width of the additively manufactured samples directly depends on the scanning speed and the powder feed rate. Scanning speed has a reverse effect on the height stability, i.e., the lower the scanning speed, the larger the stability. Microstructural results showed that because of the solidification process, the alloying elements will be accumulated in the grains boundaries. The non-uniform cooling rate and non-steady solidification rates of molten area in additive manufacturing process, the microhardness values of the additively manufactured samples following a fluctuated trend.

Keywords: Additive Manufacturing; Direct Laser Metal Deposition; Inconel 718 Superalloy; Dimensional Stability; Microstructure.

1. Introduction

The processes for additive manufacturing, also referred to as 3D printing, have advanced significantly in recent years and companies and Institutions have made a healthy rival for expanding the benefits aspects of this field of science such as cost, complex geometries, replacement and maintenance [1-4]. With the development of specialized facilities in this field of technology and providing superb conditions for the manufacturing of parts with maximum accuracy and cost-effectiveness along with rapid production, it has attracted the attention of many scholars and industries [5-7]. The additive manufacturing process is also referred to layer production [8-10]. This method is one of the fastest and most reliable manufacturing processes, which is used to create a new sample via high quality and accuracy [11]. 3D printing has many advantages over traditional production methods [12]. The production of complex geometries by means of traditional manufacturing methods is very sophisticated and is not affordable in many cases. A wide range of materials are applied for additive manufacturing approaches such as plastics, metals, ceramics, and composites [13-16]. The additive manufacturing technology is divided into different categories based on their approach of printing, equipment or printer devices, material and etc [17-20]. The laser equipment is one of the most useful equipment in the industry that plays a very important role in manufacturing lines [21-24].

The laser additive manufacturing method is a modern and evolving process, which is capable of many complex components by using a variety of powders, including metals, non-metallics and composites [25-28]. In additive manufacturing process by laser, layers are produced by various input parameters [29-30]. Recently, extensive research has been done in this field of science. Kong *et al.* [31] investigated the effect of deposition created by laser additive manufacturing process on non-traditional machining via a high-throughput dual-feed system. Wolff *et al.* [32] evaluated laser additive manufacturing by twin

feeders where Inconel 718 was used as powder. The goal of this study was that how the cooling rate after AM process can be effected on AMed samples structure. An experimental study from the additive manufacturing process of Inconel 718 which was shown the sidewall nonuniformity and deposit bulge was performed by Lee *et al.* [33]. The quality and dimensions accuracy of additively manufactured specimens were studied in references [34-38]. The results showed that this experiment provided some additively manufactured samples with a suitable surface quality. A similiar research about the quality and micro-hardness trend was conducted by Liu *et al.* [39]. It is worth mentioning that the Inconel 718 material is one of the most used materials in the manufacturing industry. Shang *et al.* [40] joined two parts of multi-material objects by the laser additive manufacturing process. Due to the joining parts of AM process some parts were joined very well. Caiazzo *et al.* [41] generated some layers by changing nozzle scanning speed and laser power in the Directed Metal Deposition (DMD) method. These parameters have a critical role in AM process because by controlling these inputs the samples were generated very well. Liu *et al.* [42] investigated Laser Powder Deposition (LPD) method by using the AlSi10Mg alloy and Taguchi approach for the optimization of additive manufacturing process. Wang *et al.* [43] studied microstructure of the deposited layer of additively manufactured samples. DLAM method in the laser additive manufacturing process for biomaterials based titanium and molibden (Ti-15Mo) was studied by Bhardwaj *et al.* [44]. With this approach, they printed some samples which are usable in human surgery parts. Momenzadeh *et al.* [45] investigated the simulation and analysis of specific implant, which was printed by the laser additive manufacturing process. AISI 304L is a very popular stainless steel in the manufacturing process. This material was joined to a Ti- 6Al-4V with the laser additive manufacturing process by Reichardt *et al.* [46]. The deposition layer from the laser additive manufacturing process via high power diode laser by AISI 316L powder was investigated in Guo

et al. [47]. The microstructure of additively manufactured parts shown that the stability between interfaces of layers was a superb joint together.

As the above review shows, the relation between direct laser metal deposition and microstructure effects after additive manufacturing of super alloys have been addressed. However, there are still many areas which have not been considered. By conducting some research, it is clear that, the behavior of the AM process on the microstructure of Inconel 718 is very sophisticated because the cooling rate and controlling the input parameters for generating a high-quality structure is very complicated. Inconel 718 is one of the much usable superalloys which its behavior from the procedures for material processing is very important in industry applications. In the present study, the DLMD process is applied for additive manufacturing of Inconel 718 nickel-base super-alloy deposited wall on the AISI 4130 alloy steel substrate using a 1kW fiber laser. The effects of powder feed rate and scanning speed on geometrical aspects (i.e. height, average of width), microstructural observations and microhardness trend of additively manufactured samples in different layers are investigated. The results are explained by powder catchment ratio concept in DLMD process. Considering the powder catchment ratio concept and studying the geometrical stability of the additively manufactured walls, are relatively new accompaniments to this field.

The organisation of the remainder of this paper is as follows. In Section 2, experimental study of DLMD process and some parameters are discussed such as catchment, stability rate, which are considered as outputs. In Section 3 and 4, results from measurements and conclusions are discussed, respectively.

2. Experimental study

In this section, the additive manufacturing process using the Inconel 718 powder via the DLMD method by 1 kW fiber laser is investigated.

2.1.Experiment set-up

The laser is a continuous wave which is embedded within a CNC table that moves in three perpendicular directions (x, y, z). The table in each direction is moved by Mach3D software that defines a special G-code for each direction of the table. When the table moves based on regulated CNC profram, the powder is deposited by the laser beam, and the additively manufactured sample is constructed (Figure 1). The powder supply on the additive manufacturing process is a twin powder feeder system. The powders are carried out by gas pressure transfers into the feeder and powder inside the vessel.

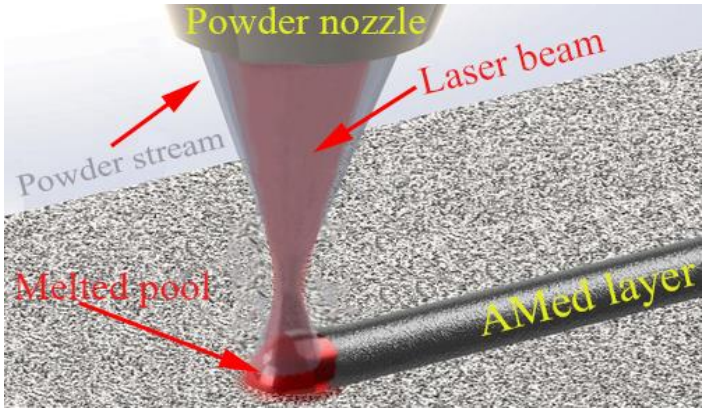

Figure 1 Laser additive manufacturing setup [48]

In this study, commercial powder of Inconel 718 is used. Figure 2 shows the FE-SEM images of the Inconel 718 powder. The particle size of the powder was photographed with a Field Emission Electron Microscopy (FE-SEM) by MIRA lll model, manufactured by TE-SCAN.

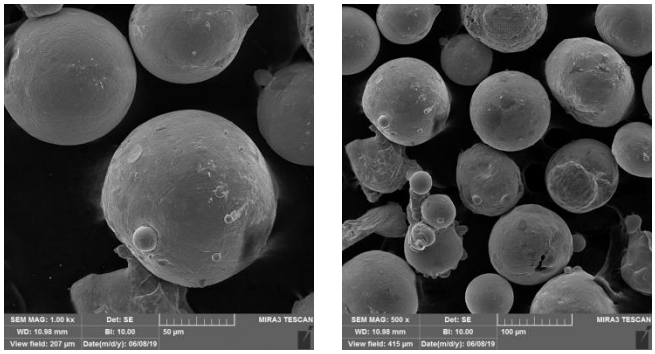

Figure 2 FESEM of Inconel 718 powder

As can be seen, the particle size of the powder is in the range of 45-90 μm. Due to previous studies and research the size of powder must be in this range. When the size of a particle smaller or larger than 40-120 μm, the quality of AMed samples may be decreased. The chemical compositions for the Inconel 718 powder and the AISI 4130 steel are given in Table 1. AISI 4130 steel was used as a substrate. Inductively Coupled Plasma Spectrometer (ICP) analysis has been applied to obtain powder compounds and quantum test for the percentage of compounds in the substrate. The substrate structure is ferrite-perlite and raw bar for AISI 4130 steel with a thickness of 7 mm and a diameter of 65 mm.

Table 1 Chemical composition (Wt. %) of Inconel 718 and AISI 4130 steel

Powder	**Inconel**	**Al**	**Co**	**Cr**	**Fe**	**Mn**	**Mo**	**Nb**	**Ni**	**Ti**
	718	0.248	0.0768	19	17.5	0.163	3.29	4.9	54	0.13
Substrate	**AISI**	**Mo**	**Cu**	**Cr**	**S**	**Mn**	**Si**	**P**	**Ni**	**C**
	4130	0.25	0.06	1.01	0.03	0.87	0.3	0.016	0.05	0.25

In this study, the argon gas is used as a shielding gas as well as the powder carrier gas. In all experiments, axial gas pressure (3 liters per minute), powder carrier gas pressure (1.5 liters per minute) and 250 W laser power were considered as constant parameters. The Focal Plane Position (FPP), the number of deposition layers (5 layers), the dwell time of the deposition layers and the continuous laser wave are also considered as fixed parameters. In addition, two parameters of this process, the powder feed rate, and CNC table scanning speed are variable. Table 2 presents the values of process input and output parameters. After the additive manufacturing process, the specimens were cut by the wire-cut, and their cross-sections were etched according to ASTM E 407: 07 by Glyceregia electrochemistry for the metallographic process [49]. The Ws in Table 2, show the width of AMed samples in three areas, top, middle, and bottom of AMed samples, respectively.

Table 2 Input and output parameters of laser additive manufacturing process

No.	Inputs		Outputs			
	Scanning speed (mm/s)	**Powder rate (gr/min)**	**W_1 (µm)**	**W_2 (µm)**	**W_3 (µm)**	**h (µm)**
#1	5	28.52	108	1280	350	3105
#2	5	17.94	862	1005	594	1912
#3	2.5	17.94	792	1253	474	2767
#4	2.5	28.52	945	1479	836	4890

Figures 3 and 4 show respectively the additively manufactured samples and their geometrical dimensions which are made by the DLMD method. In Figure 3, some parts of AMed are divided for understanding the concept of the height of samples. Also, in Figure 4, the concept of width in their zones for four samples are illustrated.

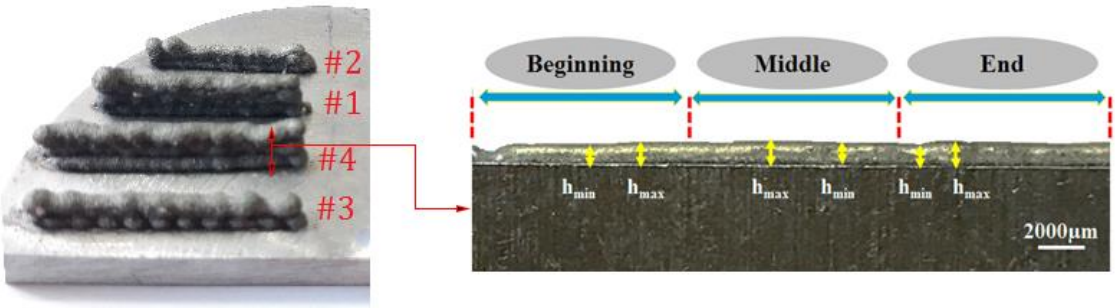

Figure 3. Additively manufactured samples and cross-section of a printed part (thickness of the substrate is 7 mm)

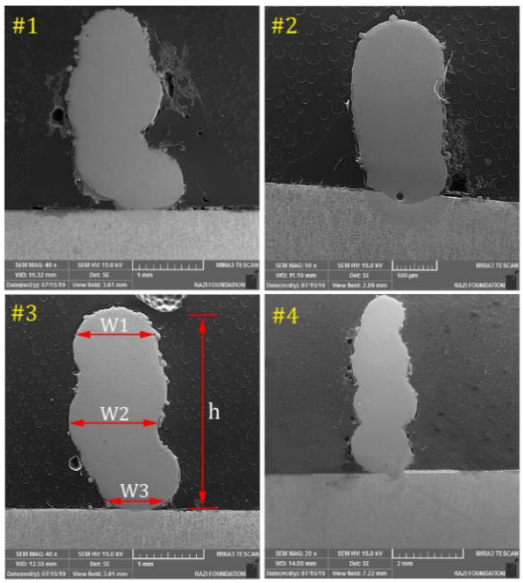

Figure 4. The macro size images of additively manufactured samples

Measurements of geometric dimensions of the specimens in four parts of deposition sections (beginning (W1), middle (W2), end of the deposition layer (W3), and the height (h)) are determined by the ImageJ software based on FE-SEM images (see Figure 4). The stability is a modern approach, and it is a suitable criteria for the height quality of deposited layers. The length of the deposited layer is divided into three sections. The maximum and minimum heights are measured, and the differences of the heights are calculated. The maximum difference is defined as stability value. A lower stability rate can be more suitable for this process because the lower amount of stability means that the differences between minimum and maximum heights are less (Figure 3). The equations related to the calaution of stability value are shown in followings:

$$\Delta h_1 = H_{max_1} - H_{min_1} \quad (1)$$

$$\Delta h_2 = H_{max_2} - H_{min_2} \quad (2)$$

$$\Delta h_3 = H_{max_3} - H_{min_3} \quad (3)$$

$$\Delta H = \text{Max}\ \{\Delta h_1, \Delta h_2, \Delta h_3\} \quad (4)$$

The microstructure images in this study were photographed by using Optical microscopy (OM) and FE-SEM. ImageJ software was used to analyze the geometric dimensions of the specimens. The Vickers micro-hardness for samples were evaluated via BUEHLER models. The specimens were tested with a loading rate of 100 gr for 30 seconds on the micro-hardness test. Powders feed focus point, spray bandwidth, and powder flow feed rate measurements were examined to characterize the powder feed conditions. To determine the powder focus point, the axial gas feed rate, powder carrier gas feed, and powder feeder rotation speed must be adjusted. This is very vital because the powder particles fed from the four outlet channels converge at one particular point. The parameters of scanning speed, distance of laser head to the substrate, and the rotation speed of powder feeder were changed to evaluate the effect of parameters. The spray bandwidth is measured by three times along the path. The mass feed rate is defined as the feed

rate of the powder passing through the powder outlet channels of the twin powder feeder. Powder mass feed rate, gas pressure, and disk powder velocity were varied to measure the mass feed rate. The lens of the fiber laser device has a ±4 mm displacement, which is related to sample position. The focal point position is at the highest point on -4 mode. Also, at the zero points, the focal point is on the substrate [15].

2.2.Catchment

The concept of catchment in additive manufacturing has an applied aspect because it shows the absorption of powder components. According to equation (5), catchment is dependent on the powder feed rate and laser scanning speed. It is expected that the catchment factor increases by increasing the powder feed rate, but the powder feed rate has a turning point. It means that the powder feed rate increases to a certain extent, but suddenly it makes a situation for absorbing more powder, and in this stage, the amount of catchment declines [50].

$$\text{Catchment} = \frac{Powder\ flow\ rate\ (gr)}{Scanning\ speed\ (mm)} \qquad (5)$$

Generally, the samples' geometry and height are dependent on three input factors, namely, powder feed rate, laser scanning speed and laser power. The melt pools can absorb more powder by increasing the powder feed rate. However, the height of samples does not sometimes change by increasing the powder feed rate, because the laser power is low and the situation for absorbing more powder is not provided in the melted pond. In the specific circumstances, the melt pool, which is created by laser irradiation, can receive and absorb more powder by increasing the powder feed rate. When the powder feed rate and the scanning speed are regulated on a constant amount, generated energy can attend to absorb a limited amount. This phenomenon means that, when the powder feed rate is in the highest rate, it cannot add any more powder to the melt pool. In addition, the uncompleted melting of powder affects samples' height because the input energy is low. Also,

Cong *et al.* [51] showed that when the powder feed rate changed from 0.1 gr/min to 0.4 gr/min, the melt pool caught more powder and finally the height of samples increased. However, the samples' height may still remain constant until the powder feed rate goes to a proper rate. This is because the laser power and scanning speed are regulated on the constant amount and the rate of powder which is absorbed by energy absorption has been limited. The focus on issues of final surface is one of the most critical limitations in the DMD process. The difference between the roughness and waviness as two specific factors in modifications of surface is proposed. Gharbi *et al.* [52] conducteded a research which showed that tiny additively manufactured layer and bier melt pool improved the quality of surface. Also, it was observed that by increasing the interaction between the powder feed and laser beam, more powder would be absorbed that is one of the most beneficial effects for the final surface. When the amount of catchment is at a high rate, the interaction between powder and laser beam increases, and finally, it makes a surface with improved quality.

3. Results and Discussion

In this section, the results of the experiments are presented and discussed. The scanning speed and powder feed rate were the input parameters, whereas the microstructure, width, height, stability, and microhardness of additively manufactured samples were the output parameters. In what follows, the effects of input parameters on the output parameters are evaluated.

3.1.Effect of catchment parameter on the wall height

According to equation (5), the catchment parameter consists of the powder feed rate and scanning speed. The scanning speed is an affecting parameter on the additively manufactured wall geometry. In this research, two different scanning speeds of 2.5 and 5 mm/sec were considered. The maximum wall height at the lowest scanning speed (i.e, 2.5 mm/sec) was observed as 4890 micron. In low

scanning speed, the powder particles have more time for deposition. On the other hand, in the high scanning speed, the powder particles have lower absorbed energy, and the additively manufactured wall height will decrease. According to Table 2, the minimum additively manufactured wall height at the highest scanning speed (i.e., 5 mm/sec) was obtained as 1912 micron. Generally, a reduction in scanning speed causes an increase in powder deposition and also wall height. In this study, two powder feed rates of 17.94 and 28.52 g/min were used. The maximum additively manufactured wall height was observed at the maximum powder feed rate (i.e., 28.52 g/min). When the powder feed rate increases, much more powder particles interact with the laser beam. The laser beam energy melted and deposited the powder particles on the substrate. The minimum additively manufactured wall height was observed at the minimum powder feed rate (i.e., 17.94 g/min). Figure 5 shows the effects of powder feed rate and scanning speed on the additively manufactured wall height. It is clear that by decreasing the scanning speed when the power rate is considered as a constant parameter, the height of the samples increased. This phenomenon completely depended on the time for the Additive process which more powder melted and the hight increased.

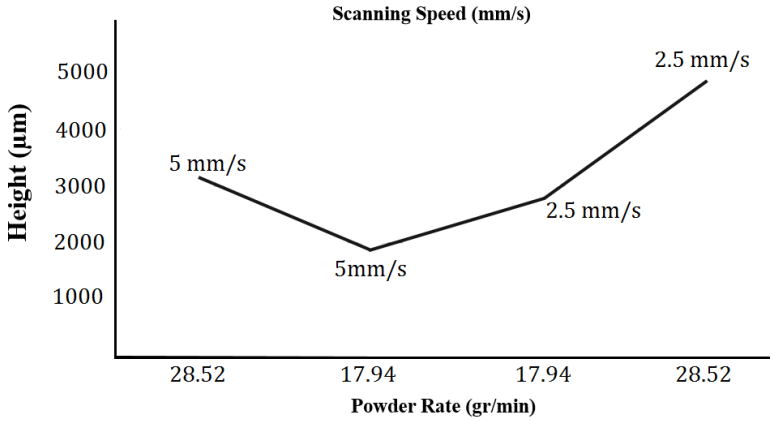

Figure 5. The effect of powder feed rate and scanning speed on wall height.

3.2.Effect of catchment parameter on the wall width

The maximum additively manufactured wall width is 1086 micron, which was observed at minimum scanning speed of 2.5 mm/min. It was found out that the lower the scanning speed the higher would be the wall width of additively manufactured samples. At a low scanning speed, the powder particles that are interacted and melted by laser beam would have more time to wider deposition, causing an increase in the wall width. The minimum wall width was 820 micron that was observed at minimum scanning speed, i.e., 2.5 mm/min. With increasing in the powder feed rate, much more powder particles feed coming out from nuzzles and it caused that, more powder interacted with the laser beam and melted. Therefore, the wall width increased. The maximum wall width of additively manufactured samples was observed at powder feed rate of 28.52 g/min.

3.3.Microstructure and microhardness analysis

The ϒ phase is the base phase in Inconel 718 superalloy called ϒ Matrix. In this superalloy, some of other phases such as ϒ′, ϒ″, δ, Metallic Carbides (MC) and Laves phases are also generated. The ϒ′ and ϒ″ phases are the main reinforcement phases and those are coherent with ϒ phase. The ϒ′ phase composition is Ni_3 (Al-Nb-Ti) and the ϒ″ phase composition is Ni_3Nb [53]. The Laves phases are not desirable in terms of mechanical properties, but the heat treatment can dissolve Laves phases into the matrix. According to Figure 6, the ϒ phase is dispersed uniformly in all over the sample microstructure and it is the gray phase. Also, from Figure 6, it is found out that the most part of the additively manufactured sample microstructure is the ϒ phase. The white areas in Figure 6-a are the Laves phases that are in irregular shapes and dispersed non-uniformly. The Laves phases are precipitated into the grains and in the grain boundaries.The dark-gray areas in Figure 6-b & c are the ⟦ϒ⟧^' phase.

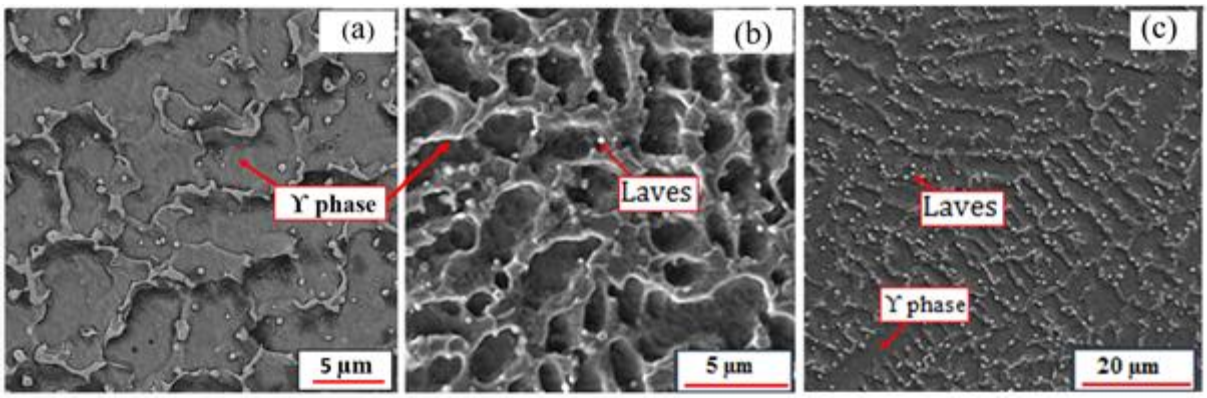

Figure 6. Inconle 718 addetived structure **a)** ϒ phase **b)** 〖ϒ〗^' phase **c)** Laves phases

The EDS analysis provides quantitative and qualitative analyses from a wide range of materials. The microanalysis from different zones of additively manufactured samples and substrate was done to achive the point chemical compositions and quantitative and qualitative analyses of phases. The different selected zones from sample #3 were illustrated in Figure 7.

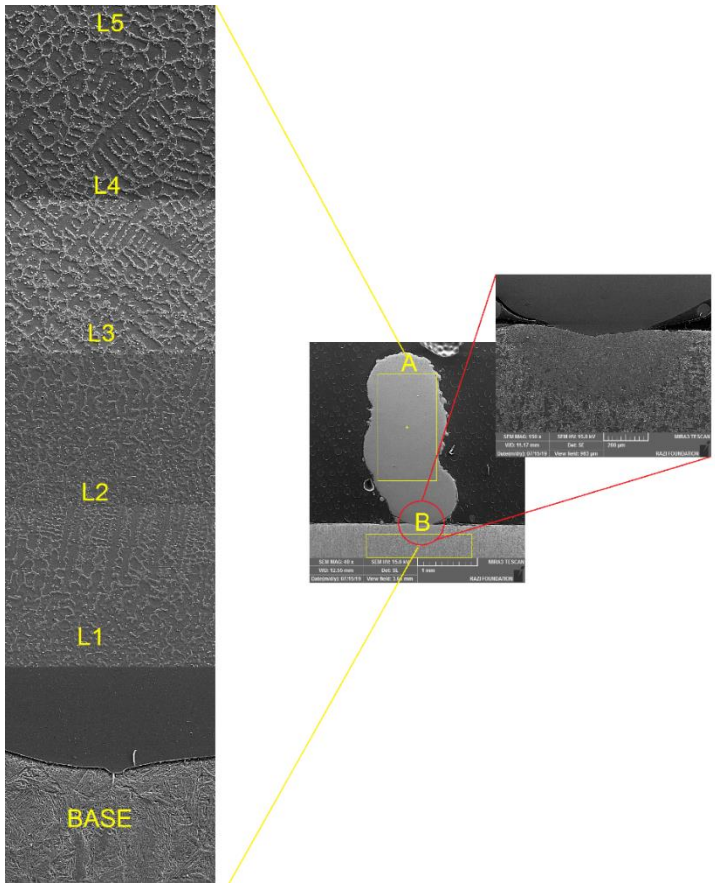

Figure 7. The EDS analysis in 5 layers (L1-L5) of addetived sample #3

Tables 4 and 5 present the chemical compositions of additively manufactured sample 3 based on atomic and weight percentages in spot A and B, respectively.

Table 4. Chemical composition (Wt. %) of sample #3 in spot A

Element	[norm. wt%]	[norm. at%]
Aluminium	0.16	0.38
Silicium	0.91	2.12
Titanium	0.33	0.32
Chromium	16.53	20.24
Iron	14.8	17.22
Nickel	51.75	48.50
Niobium	4.92	3.47
Molybdenum	3.3	2.53
Aurum	7.3	5.22
Sum	**100**	**100**

Table 5. Chemical composition (Wt. %) of sample #3 in spot B

Element	[norm. wt%]	[norm. at%]
Carbon	6.67	25.21
Silicium	0.36	0.58
Chromium	0.79	0.69
Iron	87.84	71.46
Molybdenum	4.34	2.06
Sum	100	100

The Map analysis provides the frequent distribution of elements in an image. In any area where the color intensity is higher, it indicates that the percentage of the element in that area is higher. Figure 8 shows the Map analysis of sample number 4. The elements distribution in the Inconel 718 additively manufactured samples were illustrated in different colors. According to ICP analysis, the most parts of the elemental composition of Inconel 718 powder included the Ni, Cr, Fe, Nb, and Mo elements. The main elements of powder particles were Ni, Cr, and Fe by the weight percentages of 54%, 19% and 17.5%, respectively. The Map images showed the uniform distribution of Ni, Co, Cr, and Ti elements all over the sample. The brighter spots in the Map images indicate the more intensity of elements distribution. The Al, Nb, Mo, and Si elements are distributed non-uniformly and accumulated in grains boundaries. The Laves phases will be precipitated in the grain boundaries. The atomic percentage of Nb and Mo

elements are higher in the Laves phases than the other phases, thus the Nb and Mo elements were accumulated in grains boundaries. During the DLMD process, the powders melted. The elements are uniformly distributed in the molten materials, but during the solidification process, the alloying elements will be accumulated in the grains boundaries. In the Inconel 718 alloy, both the Nb and Mo elements are susceptible to separation due to the small redistribution coefficient (<1), which causes a non-uniformity distribution of the alloy composition in the solid-liquid interface.

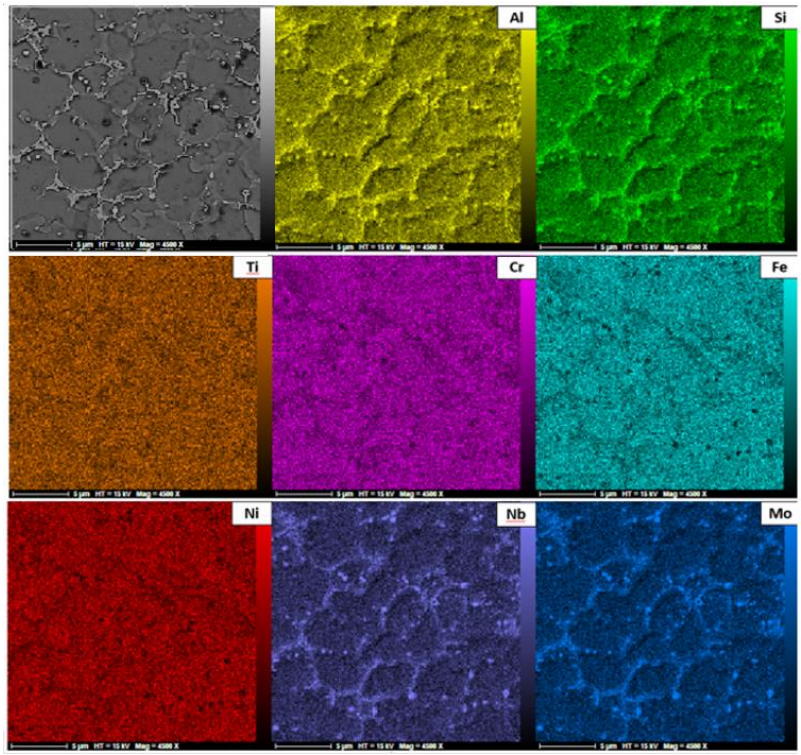

Figure 8. Map analysis of sample number 4.

The grain morphology of Inconel 718 is diverse in different regions. Columnar dendrites, cellular dendrites, cells, and equiaxial dendrites with Laves phases are observed in the interdendritic areas. Generally, the grain growth was epitaxial, but in some areas, the dendritic growth was observed. The dendrites were grown along of the deposition layer direction. The Microstructure of Inconel 718 is columnar dendrites growing epitaxially along the deposition direction. Figure 9 shows the FE-SEM images for samples number 1 to 4. The columnar

growth was observed, and in some areas, the grains were more extensive and more stretched.

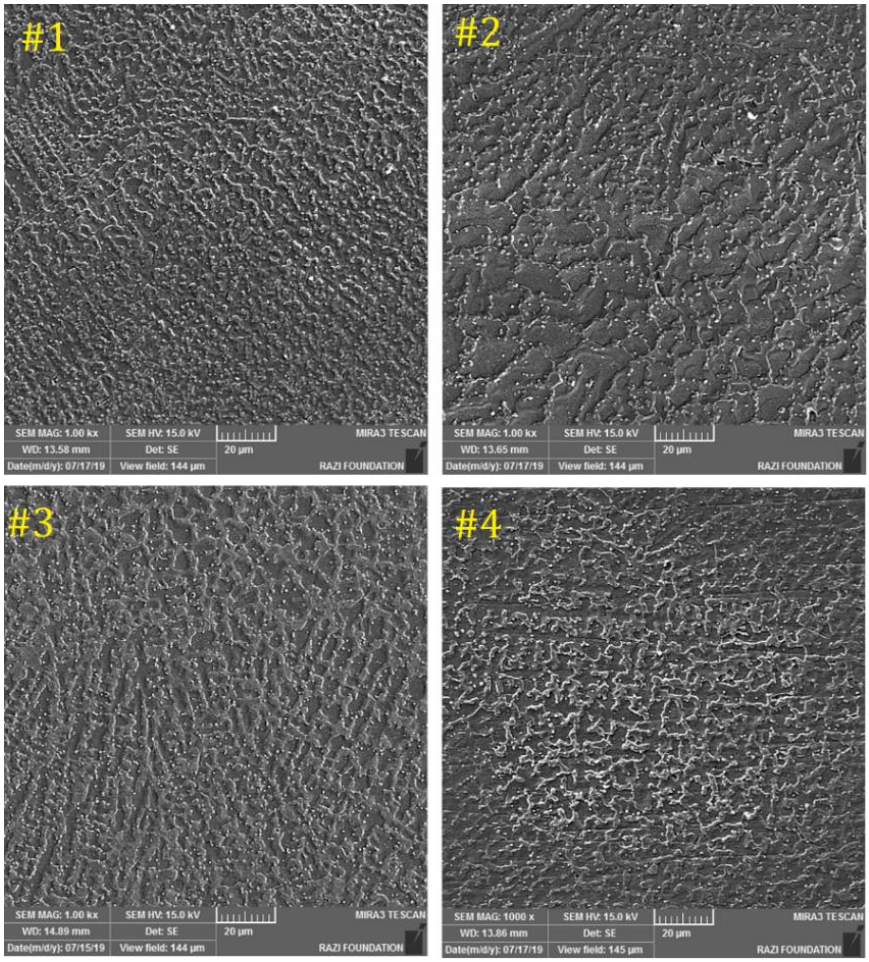

Figure 9. FE-SEM of samples number 1 to 4.

The orientation of grains changed in the areas near to the substrate. The substrate acts as a heat source for the first layers of deposited wall, and large columnar dendrites were grown. When laser energy melted the new layer, it simultaneously affected an earlier layer and caused grain growth in previous layer. The grain growth would occur due to increase in temperature and reheating the layer. Figure 10 showed the growth in grain size in the overlap zone of two layers.

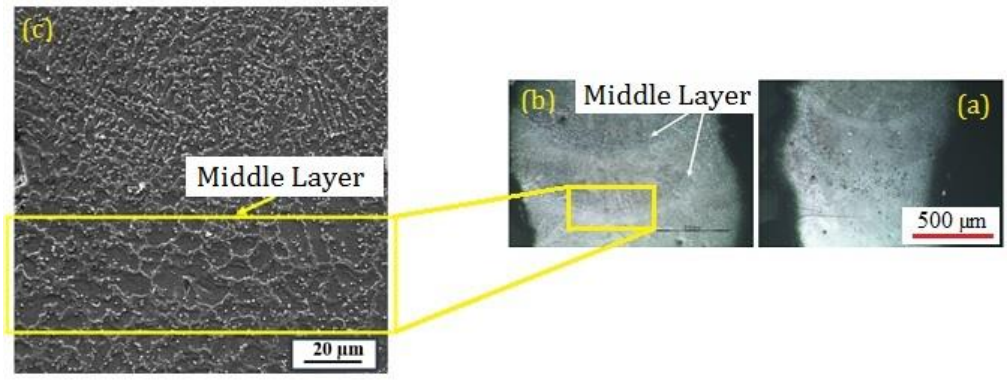

Figure 10. The common boundary between the deposit layers.

The heat input of the laser beam from the upper layer is affected by the interfaces of layers, and the grains are grown. Figure 11 shows the microstructure of samples number 1 and 4. The laser power was 250 W. Thus, the heat input changed due to the alteration of scanning speeds. When adding melted upper layer to the hardened layer or lower layer, the solidified layer was affected by heat input caused from the upper layer. Therefore, grains of lower layers were grown. A high laser power leads to a deeper melt pool, whereas a low scanning speed causes much more powder particles to be deposited in the melt pool. Therefore, at low scanning speed, strong joints between layers are created, and it will avoid cracking and separating in the interfaces.

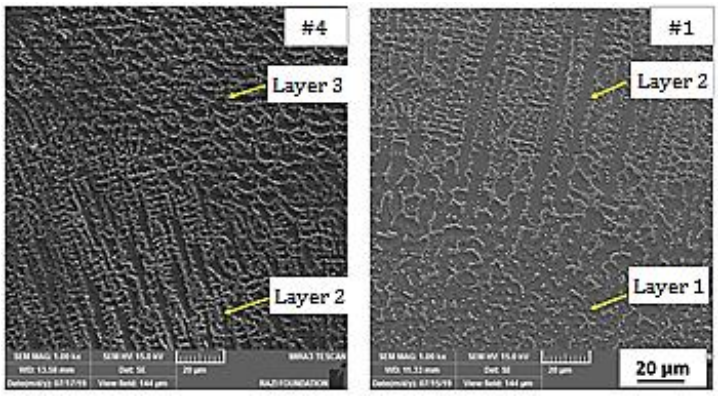

Figure 11. The common boundary layer of samples number 1 and 4.

In Figure 12, the equiaxed dendritic microstructures at the surface of deposition were illustrated. With increasing in the additively manufactured wall height, the grains orientation in top section of samples is differed from the parts,

which are near to the substrate. The columnar microstructure with equiaxed dendrites showed that changes in the microstructure is caused by the changing solidification conditions at top of the deposition. In the top sections of samples, the columnar grains and equiaxed dendrites were created due to low-temperature gradients and high solidification speed [54-56].

The top of the workpiece after the deposition of the melted substrate could be quenched by air. However, the bottom of the melted substrate is quenched by thermal transformation to the lower layer, which is addetived before. Furthermore, in the top sections of additively manufactured samples, the molten powder particles interacted with shielding gas. Thus, the solidification velocity increased. The convection heat transfer between the last solidified layer and shielding gas was occurred in top layers of additively manufactured samples, while in the lower layers, the conduction heat transfer between additively manufactured layers and previous layers have occurred.

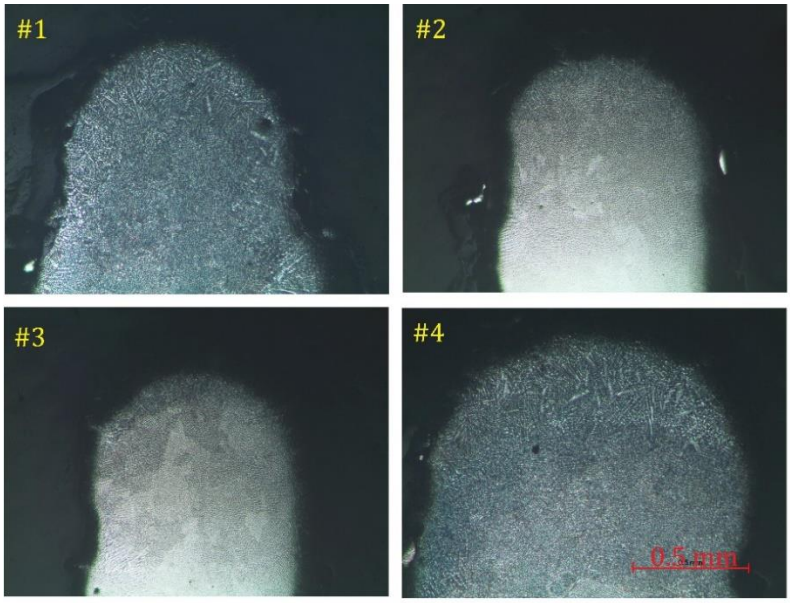

Figure 12. Top section microstructure of the additively manufactured samples for samples #1 to #4

The additively manufactured samples may have some defects, such as porosity, open pores, and shirinkage cavities. The porosity and unmelted powders are the usual defects that may happen during the additive manufacturing process. In Figure 13, it is shown that the closed and open pores are the black spots. The

porosity of the additively manufactured samples is due to the powder quality and excessive pressure of shielding gas flow [57]. The powder particles quality depends on powder production methods. The powders produced by Plasma Rotating Electrode Process (PREP) and Gas Atomization (GA) methods are better powders than the other powder production methods for reducing the porosity in the additively manufactured samples. In this research, Inconel 718 powder particles were gas atomized and made lower porosity in the additively manufactured samples.

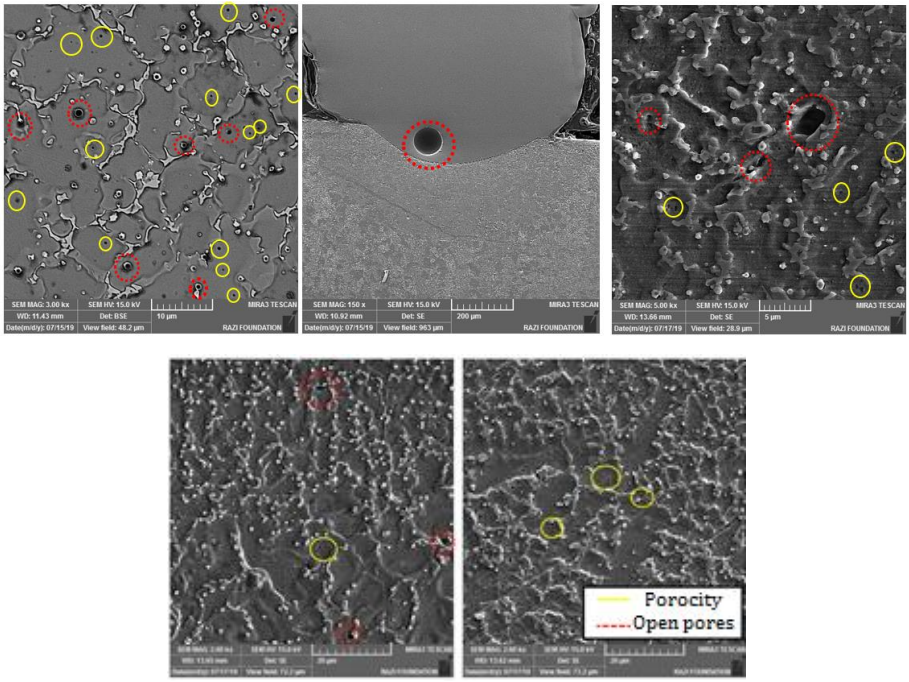

Figure 13. Defects in the microstructure of the addetived samples

The values of Vickers microhardness of samples number 1 and 4 from top to bottom are illustrated in Figure 14. The microhardness values of the additively manufactured samples following a fluctuated trend. Based on the non-uniform cooling rate and non-steady solidification rates of molten Inconel 718 during the additive manufacturing process. It is due to the heat input from upper layers that affected the lower layer, and changed the microstructure, grain size as well as microhardness. In other words, the heat input from the upper additively manufactured layer led to an increase in microhardness of lower additively

manufactured layers. It is worth mentioning that the morphology and concentration of the Laves phase were found to be the most critical factors in the microstructure of Inconel 718 alloy. On the other hand, as mentioned in section 3.2, the Laves phase is not a hard phase. The Laves phase is the Nb-rich phase in the ϒ matrix (see Figures 6 and 8). Accordingly, the precipitation of the Laves phase reduced the microhardness of the additively manufactured samples.

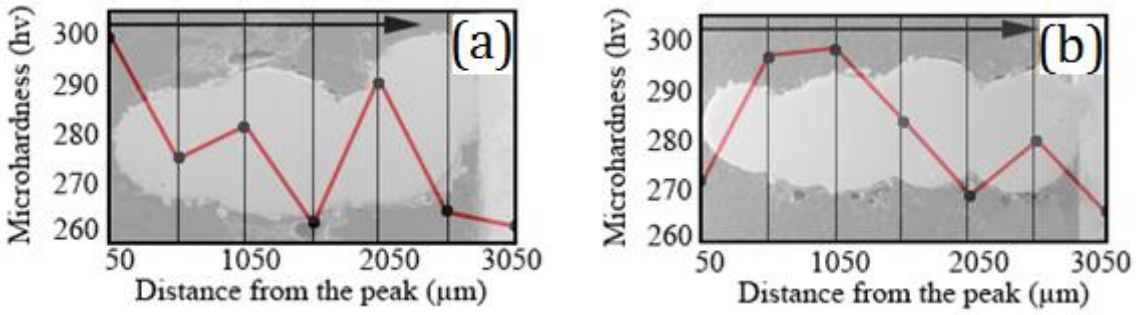

Figure 14. Microhardness of samples a) number 1 and b) number 4.

4. Conclusions

In this study, the influence of two effective parameters on the direct laser metal deposition of additive manufacturing process for Inconel 718 superalloy was examined. The results showed that the powder feed rate and scanning speed have an effectual impact on the additively manufactured samples features. The following conclusions are made:

1. The height of the samples depends on two main factors, namely, scanning speed and powder feed rate. When the scanning speed decreases, the laser's interaction time with the powder particles increases, which leads to a higher additively manufactured wall height.
2. The average width of the deposited layer depends on the scanning speed and the powder feed rate. By declining the scanning speed to 2.5 mm/s, the deposition from the melted powder having more time for going wider width and is developed to 1479 μm on bottom of workpieces.

3. Height stability is an important parameter in measuring the quality of the additively manufactured samples. A low ΔH value means that the difference between the highest and the lowest heights of the sample is lower. The lowest ΔH, which has proper stability, is obtained in the less scanning speed.
4. Change of micro-hardness in the samples does not follow any specific trend. The microstructural changes along with the height of a sample by DLMD. The heat input from the upper layers that affected the lower layer and the laser heat input acts as a heat treatment.
5. Various phases with different grain growth morphology in different parts of additively manufactured samples are generated which cause fluctuiation in microhardness regims.
6. In DLMD of Inconel 718 superalloy, during the solidification process, the alloying elements such as: Nb and Mo, will be accumulated in the grains boundaries. The Laves phases are Nb and Mo rich phases, thus the Laves phases will be precipitated in the grain boundaries. The Laves phases are not desirable in terms of echanical properties.

References

[1]. T. D. Ngoa, A. Kashania, G. Imbalzanoa, K. T.Q. Nguyena, D. Huib, (2018). Additive manufacturing (3D printing): A review of materials, methods, applications and challenges. *Composites Part B* (143), 172–196.

[2]. J. C. Najmon, S. Raeisi, A. Tovar, (2019). Review of additive manufacturing technologies and applications in the aerospace industry, *Additive Manufacturing for the Aerospace Industry*, 7-31.

[3]. H. Bikas, P. Stavropoulos, G. Chryssolouris, (2016). Additive manufacturing methods and modeling approaches: a critical review. *Advanced Manufacturing Technology*, 83(1-4), 389-405.

[4]. D. Clark, M. T.Whittaker, M. R.Bache, (2012). Microstructural characterization of a prototype titanium alloy structure processed via direct laser deposition (DLD). *Metallurgical and Materials Transactions B*, 43(2), 388-396.

[5]. M. Moradi, S. Meiabadi, A. Kaplan, (2019). 3D Printed Parts with Honeycomb Internal Pattern by Fused Deposition Modelling; Experimental Characterization and Production Optimization. *Metals and Materials International*, 25 (5), 1312-1325.

[6]. Y. Yang, Dongdong Gu, D. Dai, C. Ma, (2018). Laser energy absorption behavior of powder particles using ray tracing method during selective laser melting additive manufacturing of aluminum alloy, *Materials & Design*, 143, 12-19.

[7]. I. F.Ituartea, N. Boddetib, V. Hassanib, M. L. Dunnb, D. W. Rosenb,(2019), Design and additive manufacture of functionally graded structures based on digital materials, *Additive Manufacturing*, 30, 100839.

[8] Moradi, M., Karami Moghadam, M. and Asgari, F., (2020). 4D printing additive manufacturing review; Mechanisim, Chalanges, Applications and Future, *Modares Mechanical Engineering*, 20(4), 1063-1077.

[9]. S. M. Thompson, L. Bian, N. Shamsaei, A. Yadollahi, (2015). An Overview of Direct Laser Deposition for Additive Manufacturing Part I: Transport Phenomena, Modeling and Diagnostics, *Additive Manufacturing*, 8, 36-62.

[10] Moradi, M., Karami Moghadam, M., Shamsborhan, M. and Bodaghi, M., 2020. The Synergic Effects of FDM 3D Printing Parameters on Mechanical Behaviors of Bronze Poly Lactic Acid Composites. *Journal of Composites Science*, 4(1), 17.

[11]. N. Shamsaeia, A. Yadollahia, L. Bianc, S. M. Thompsona, (2015). An overview of Direct Laser Deposition for additive manufacturing; Part II: Mechanical behavior, process parameter optimization and control, *Additive Manufacturing*, 8, 12-35.

[12]. T.E. Abioye, P. K. Farayibi, A.T. Clare, (2017). A Comparative Study of Inconel 625 Laser Cladding by Wire and Powder Feedstock, *Materials and Manufacturing Processes*, 32(14), 1653-1659.

[13]. T.E. Abioye, D.G. McCartney, A.T. Clarea, (2017). Laser cladding of Inconel 625 wire for corrosion protection, *Materials Processing Technology*, 217, 232–240.

[14]. T. E. Abioye, A. Medrano-Tellez, P. K. Farayibi, P. K. Oke,(2017). Laser Metal Deposition of Multi-Track Walls of 308LSi Stainless Steel, *Materials and Manufacturing Processes*, 32(14), 1660-1666.

[15] Moradi, M., Ashoori, A., & Hasani, A. (2020). Additive manufacturing of stellite 6 superalloy by direct laser metal deposition–Part 1: Effects of laser power and focal plane position. *Optics & Laser Technology*, 106328.

[16] Moradi, M.; Karami Moghadam, M.; Shamsborhan, M.; Bodaghi, M.; Falavandi, H., (2020). Post-Processing of FDM 3D-Printed Polylactic Acid Parts by Laser Beam Cutting. *Polymers*, 12, 550.

[17] Moradi, M., Falavandi, H., Karami Moghadam, M., Meiabadi, S.M. and Saleh, M., (2020). Experimental Investigation on Laser Cutting Post Process of Additive Manufactured Parts of Poly Lactic Acid (PLA) by 3D Printers Using FDM Method. *Modares Mechanical Engineering*, 20(4), 999-1009.

[18] Li, W., Yan, L., Karnati, S., Liou, F., Newkirk, J., Taminger, K. M. B., & Seufzer, W. J. (2017). Ti-Fe intermetallics analysis and control in joining titanium alloy and stainless steel by Laser Metal Deposition. *Journal of Materials Processing Technology*, 242, 39-48.

[19] Angelastro, A., Campanelli, S. L., & Casalino, G. (2017). Statistical analysis and optimization of direct metal laser deposition of 227-F Colmonoy nickel alloy. *Optics & Laser Technology*, 94, 138-145.

[20] Caiazzo, F., Alfieri, V., Argenio, P., & Sergi, V. (2017). Additive manufacturing by means of laser-aided directed metal deposition of 2024 aluminium powder: investigation and optimization. *Advances in Mechanical Engineering*, 9(8), 1687814017714982.

[21] Savitha, U., Srinivas, V., Reddy, G. J., Gokhale, A. A., & Sundararaman, M. (2018). Additive laser deposition of YSZ on Ni base superalloy for thermal barrier application. *Surface and Coatings Technology*, 354, 257-267.

[22] Donadello, S., Motta, M., Demir, A. G., & Previtali, B. (2019). Monitoring of laser metal deposition height by means of coaxial laser triangulation. *Optics and Lasers in Engineering*, *112*, 136-144.

[23] Liu, W., & DuPont, J. N. (2003). Fabrication of functionally graded TiC/Ti composites by laser engineered net shaping. *Scripta materialia*, *48*(9), 1337-1342.

[24] Sahasrabudhe, H., Harrison, R., Carpenter, C., & Bandyopadhyay, A. (2015). Stainless steel to titanium bimetallic structure using LENS™. *Additive Manufacturing*, *5*, 1-8.

[25] Lima, D. D., Mantri, S. A., Mikler, C. V., Contieri, R., Yannetta, C. J., Campo, K. N., & Banerjee, R. (2017). Laser additive processing of a functionally graded internal fracture fixation plate. *Materials & Design*, *130*, 8-15

[26] Heer, B., & Bandyopadhyay, A. (2018). Compositionally graded magnetic-nonmagnetic bimetallic structure using laser engineered net shaping. *Materials Letters*, *216*, 16-19.

[27] Zhang, Y., & Bandyopadhyay, A. (2018). Direct fabrication of compositionally graded Ti-Al2O3 multi-material structures using Laser Engineered Net Shaping. *Additive Manufacturing*, *21*, 104-111.

[28] Morrow, B. M., Lienert, T. J., Knapp, C. M., Sutton, J. O., Brand, M. J., Pacheco, R. M., & Gray, G. T. (2018). Impact of defects in powder feedstock materials on microstructure of 304L and 316L stainless steel produced by additive manufacturing. *Metallurgical and Materials Transactions A*, *49*(8), 3637-3650.

[29] Prashanth, K. G., Shahabi, H. S., Attar, H., Srivastava, V. C., Ellendt, N., Uhlenwinkel, V., & Scudino, S. (2015). Production of high strength Al85Nd8Ni5Co2 alloy by selective laser melting. *Additive Manufacturing*, *6*, 1-5.

[30] Matilainen, V. P., Piili, H., Salminen, A., & Nyrhilä, O. (2015). Preliminary investigation of keyhole phenomena during single layer fabrication in laser additive manufacturing of stainless steel. *Physics Procedia*, *78*, 377-387.

[31] Kong, D., Dong, C., Ni, X., Zhang, L., Man, C., Zhu, G., & Li, X. (2019). Effect of TiC content on the mechanical and corrosion properties of Inconel 718 alloy fabricated by a high-throughput dual-feed laser metal deposition system. *Journal of Alloys and Compounds*, *803*, 637-648.

[32] Wolff, S. J., Gan, Z., Lin, S., Bennett, J. L., Yan, W., Hyatt, G., & Cao, J. (2019). Experimentally validated predictions of thermal history and microhardness in laser-deposited Inconel 718 on carbon steel. *Additive Manufacturing*, *27*, 540-551.

[33] Lee, Y. S., & Farson, D. F. (2016). Surface tension-powered build dimension control in laser additive manufacturing process. *The International Journal of Advanced Manufacturing Technology*, *85*(5-8), 1035-1044.

[34] Shamsaei, N., Yadollahi, A., Bian, L., & Thompson, S. M. (2015). An overview of Direct Laser Deposition for additive manufacturing; Part II: Mechanical behavior, process parameter optimization and control. *Additive Manufacturing*, *8*, 12-35.

[35] Zhong, C., Kittel, J., Gasser, A., & Schleifenbaum, J. H. (2019). Study of nickel-based super-alloys Inconel 718 and Inconel 625 in high-deposition-rate laser metal deposition. *Optics & Laser Technology*, *109*, 352-360.

[36] Petrat, T., Brunner-Schwer, C., Graf, B., & Rethmeier, M. (2019). Microstructure of Inconel 718 parts with constant mass energy input manufactured with direct energy deposition. *Procedia Manufacturing*, *36*, 256-266.

[37] Li, S., Xiao, H., Liu, K., Xiao, W., Li, Y., Han, X., & Song, L., (2017). Melt-pool motion, temperature variation and dendritic morphology of Inconel 718 during pulsed-and continuous-wave laser additive manufacturing: A comparative study. *Materials & Design*, *119*, 351-360.

[38] Liu, Z., Kim, H., Liu, W., Cong, W., Jiang, Q., & Zhang, H. (2019). Influence of energy density on macro/micro structures and mechanical properties of as-deposited Inconel 718 parts fabricated by laser engineered net shaping. *Journal of Manufacturing Processes*, *42*, 96-105.

[39] Liu, Z., Li, T., Ning, F., Cong, W., Kim, H., Jiang, Q., & Zhang, H. (2019). Effects of

deposition variables on molten pool temperature during laser engineered net shaping of Inconel 718 superalloy. *The International Journal of Advanced Manufacturing Technology*, *102*(1-4), 969-976.

[40] Shang, C., Xu, G., Wang, C., Yang, G., & You, J. (2019). Laser deposition manufacturing of bimetallic structure from TA15 to inconel 718 via copper interlayer. *Materials Letters*, 252, 342-344.

[41] Caiazzo, F. (2018). Laser-aided Directed Metal Deposition of Ni-based superalloy powder. *Optics & Laser Technology*, 103, 193-198.

[42] Liu, Y., Liu, C., Liu, W., Ma, Y., Tang, S., Liang, C., & Zhang, C. (2019). Optimization of parameters in laser powder deposition AlSi10Mg alloy using Taguchi method. *Optics & Laser Technology*, 111, 470-480.

[43] Wang, T., Zhu, Y. Y., Zhang, S. Q., Tang, H. B., & Wang, H. M. (2015). Grain morphology evolution behavior of titanium alloy components during laser melting deposition additive manufacturing. *Journal of Alloys and Compounds*, 632, 505-513.

[44] Bhardwaj, T., Shukla, M., Paul, C. P., & Bindra, K. S. (2019). Direct energy deposition-laser additive manufacturing of titanium-molybdenum alloy: Parametric studies, microstructure and mechanical properties. *Journal of Alloys and Compounds*, 787, 1238-1248.

[45] N. Momenzadeh, N., Rahmati, S., Azari, A. (2015). Design, Simulation and Analysis of a novel customized dental implant using Additive Manufacturing Technology, *I. J. of Manufacturing Engineering*, 2, 52-58.

[46] Reichardt, 44A., Dillon, R. P., Borgonia, J. P., Shapiro, A. A., McEnerney, B. W., Momose, T., & Hosemann, P., (2016). Development and characterization of Ti-6Al-4V to 304L stainless steel gradient components fabricated with laser deposition additive manufacturing. Materials & Design, 104, 404-413.

[47] Guo, P., Zou, B., Huang, C., Gao, H. (2017). Study on microstructure, mechanical properties and machinability of efficiently additive manufactured AISI 316L stainless steel by high-power direct laser deposition. *Journal of Materials Processing Technology*, 240, 12-22.

[48] Pinkerton, A. J. (2015). Advances in the modeling of laser direct metal deposition. *Journal of laser applications*, 27(S1), S15001.

[49] George F. Vander Voort, ASM Handbook Volume 9: Metallography and Microstructures, *The materials information company*, 1992.

[50] Moradi, M., Hasani, A., Beiranvand, Z.M. and Ashoori, A., (2020). Additive manufacturing of stellite 6 superalloy by direct laser metal deposition–Part 2: Effects of scanning pattern and laser power reduction in differrent layers. *Optics & Laser Technology*, 106455.

[51] Hu, Y., Wang, H., Ning, F., & Cong, W., (2016). Laser engineered net shaping of commercially pure titanium: effects of fabricating variables. In International Manufacturing Science and Engineering Conference, *American Society of Mechanical Engineers*, 49897, V001T02A035.

[52] Gharbi, M., Peyre, P., Gorny, C., Carin, M., Morville, S., Le Masson, P. & Fabbro, R. (2013). Influence of various process conditions on surface finishes induced by the direct metal deposition laser technique on a Ti–6Al–4V alloy. *Journal of materials processing technology*, 213(5), 791-800.

[53] Liu, F., Lin, X., Yang, G., Song, M., Chen, J., & Huang, W. (2011). Microstructure and residual stress of laser rapid formed Inconel 718 nickel-base superalloy. *Optics & laser technology*, 43(1), 208-213.

[54] Baeslack, W. A., and Nelson, D. E. (1986). Morphology of weld heat-affected zone liquation in cast alloy 718, *Metallography*, 19(3), 371–379.

[55] Gäumann, M., Henry, S., Cleton, F., Wagniere, J. D., & Kurz, W. (1999). Epitaxial laser metal forming: analysis of microstructure formation. *Materials Science and Engineering: A*, 271(1-2), 232-241.

[56] S. Sui, J. Chen, Z. Li, H. Li, X. Zhao, and H. Tan, (2020). Investigation of dissolution behavior of laves phase in inconel 718 fabricated by laser directed energy deposition, *Addit. Manuf.*, 32, 101055.

[57] Gäumann, M., Bezencon, C., Canalis, P., & Kurz, W. (2001). Single-crystal laser deposition of superalloys: processing–microstructure maps. *Acta materialia*, 49(6), 1051-1062.